Two-dimensional expansion of a condensed dense Bose gas

E.S. Annibale, A. Gammal, Klaus G. Ziegler

Angaben zur Veröffentlichung / Publication details:

Annibale, E.S., A. Gammal, and Klaus G. Ziegler. 2015. "Two-dimensional expansion of a condensed dense Bose gas." *Physica D: Nonlinear Phenomena* 307: 77–81. https://doi.org/10.1016/j.physd.2015.05.014.

Two-dimensional expansion of a condensed dense Bose gas

E.S. Annibale [a,b], A. Gammal [a,*], K. Ziegler [b]

[a] *Instituto de Física, Universidade de São Paulo, 05508-090, São Paulo, Brazil*
[b] *Institut für Physik, Universität Augsburg, D-86135, Augsburg, Germany*

1. Introduction

Many interesting features of a trapped Bose gas are described by the Gross–Pitaevskii (GP) equation. This includes dynamical studies of the Bose–Einstein condensate (BEC), such as the expansion of a BEC after switching off the trapping potential or the interference of two separate BEC's, has been performed with remarkable accuracy [1]. The GP equation provides the macroscopic quantum state of the condensed part of the Bose gas. It can be derived from a microscopic statistical model of many-body states at temperature T in the limit $T = 0$ by a saddle-point approximation. However, the GP equation is restricted to a dilute Bose gas, with less then one particle in the scattering volume. More recent experiments with optical lattices have revealed that a much richer physics appears in a dense (or strongly interacting) Bose gas [2]. The idea is that a static periodic potential of the optical lattice is provided by counter-propagating Laser fields, where particles occupy the local minima of the periodic potential. As soon as there is more than one particle per minimum the Bose gas must be considered as strongly interacting. An immediate effect of stronger interaction is the depletion of the condensate caused by the collision of particles. This is also known from the famous example of interacting bosons in form of superfluid helium. If the density of the Bose gas increases further we can even destroy the condensate completely and create a new quantum state in the form of a Mott insulator. In contrast to a BEC, the Mott insulator is characterized by local conservation of the particle number (i.e. $n = 1, 2, \ldots$ particles per minimum of the optical lattice) but without phase coherence. In a trapped Bose gas, contrary to a translational invariant Bose gas, both states can co-exist in the same system, which is known as the wedding-cake structure: at commensurate densities the system is in a Mott state with constant density and at incommensurate densities the system is in a Bose–Einstein condensed state with spatially changing density.

These strongly interacting systems cannot be described within the GP approach because the latter only takes into account the condensate and neglects the interaction with non-condensed particles. In particular, depletion of the condensate or the formation of a Mott insulating state is not accessible by the GP approach. This problem has been addressed in a number of different approaches [3,4]. A very direct approach is an extension of the GP equation that is able to take into account the interaction with the

* Corresponding author.
E-mail addresses: annibale@if.usp.br (E.S. Annibale), gammal@if.usp.br (A. Gammal), klaus.ziegler@physik.uni-augsburg.de (K. Ziegler).

non-condensed particles. It is known as the slave-boson (SB) approach and provides also a nonlinear Schrödinger equation for the macroscopic quantum state of the condensed part of the Bose gas. The interaction with the non-condensed particles leads to a modified nonlinearity though. For a dilute Bose gas the nonlinearity is the same as that of the GP equation but in the regime of the dense Bose gas it is weaker than that of the GP equation. The equation of the strongly interacting Bose gas also indicates the disappearance of the condensate when we approach the Mott-insulating state at higher density. Previous studies of a dense trapped Bose gas have shown that the BEC can be completely destroyed at the trapping center due to depletion at higher densities [5–8]. On the other hand, the vortex structure is not much affected in the strongly interacting system because the density of the condensate is low in the vicinity of the vortex core [9].

The two-dimensional expansion of a dilute BEC past an obstacle is a subject of intensive theoretical and experimental studies. A relevant parameter in these studies is the Mach number M. It is defined as the ratio of the asymptotic velocity of the flow to the sound velocity in the medium [10]. For subsonic Mach numbers in the range $0.5 \lesssim M \lesssim 0.9$, it was reported the generation of pairs of vortices and antivortices [11]. In case of a supersonic flow, the generation of oblique dark solitons inside, and Kelvin ship waves outside the Mach cone (imaginary lines drawn from the obstacle at angles $\pm \arcsin(1/M)$ with the horizontal axis) were found [12–16]. It was shown in [17] that these dark solitons are convectively unstable for large enough flow velocity ($M \gtrsim 1.5$), i.e., practically stable in the region around the obstacle. A general theory on dispersive shock waves for supersonic flow past an extended obstacle was developed in [18] and a review paper on dark solitons in BEC can be found at [19]. Experiments addressing this problem were described in [20–22]. Recently, a renewed theoretical interest in this issue was brought by the observation of an alternating vortex emission for a suitable set of parameters. These are analogous to the "von Kármán vortex street" in classical dissipative fluids [23].

In this paper we shall study the effect of the interaction between the BEC and the non-condensed particles in a dynamical situation, where a BEC is released from a parabolic trap and passes an obstacle. The obstacle is modeled by an impenetrable disk. Due to a complex interference the macroscopic wave function will experience strong density fluctuations. The results of our numerical simulation, based on the strongly interacting gas (SIG) equation, will be compared with previous calculations, based on the GP equation. The paper is organized as follows: We briefly introduce the SIG equation and compare it with GP equation. Then we present the results of our numerical simulation for an expanding cloud in two dimensions that passes an obstacle. Finally, we discuss these results and compare them with those of the GP approach.

2. Slave-boson approach

We start from a Bose gas with hard-core interaction of a given radius a, representing an effective scattering length. Then the Bose gas can be approximated by a lattice gas with lattice constant a. In other words, a provides the shortest relevant length scale in our Bose gas. This scale remains in the Bose gas even after its release from the trap. In general, a strongly interacting Bose gas has two constituents, namely condensed particles and non-condensed particles. This is the case even at zero temperature. The interplay of all these particles can be described by the slave-boson approach [5–9]. Although this is a many-body picture, the macroscopic wave function of the condensate is extracted by a variational procedure with respect to the density of the condensate analogous to the derivation of the GP equation from the weakly interacting many-body Bose gas model. The corresponding effective Hamiltonian of the macroscopic condensate state $\Phi(\mathbf{r})$ is

$$H_\Phi = -\frac{Ja^2}{6}\,\Delta + J\,(\alpha_1 - \alpha_2\chi)\,, \tag{1}$$

where Δ is the three-dimensional Laplacian. Moreover, χ is a term that is nonlinear in $|\Phi|^2$:

$$\begin{aligned}\chi(\mathbf{r}) &= \frac{\partial \log Z(\mathbf{r})}{\partial |\Phi(\mathbf{r})|^2} \\ &= \frac{1}{2}\frac{1}{Z(\mathbf{r})}\int_{-\infty}^{\infty} e^{-\varphi^2}\;\frac{\cosh\gamma(\mathbf{r})}{\gamma(\mathbf{r})^2} - \frac{\sinh\gamma(\mathbf{r})}{\gamma(\mathbf{r})^3}\;\;d\varphi,\end{aligned} \tag{2}$$

where $Z(\mathbf{r})$ is the integral expression

$$Z(\mathbf{r}) = \int_{-\infty}^{\infty} e^{-\varphi^2}\,\frac{\sinh\gamma(\mathbf{r})}{\gamma(\mathbf{r})}d\varphi \tag{3}$$

with

$$\gamma(\mathbf{r}) = \sqrt{\left(\varphi + \mu/2\right)^2 + |\Phi(\mathbf{r})|^2}. \tag{4}$$

The coefficients are $\alpha_1 = 1+\alpha$, $\alpha_2 = \alpha(1+1/\alpha^2)$, where α is a numerical constant $\alpha \approx 1/5.5$ [5,9]. The kinetic energy parameter J is associated with the mass of the bosons m by the relation

$$\frac{Ja^2}{6} = \frac{\hbar^2}{2m}.$$

All model parameters are measured in terms of the length scale a and the energy scale J. The dimensionless parameter μ is a one-particle chemical potential that is associated with the density of bosons. This can be understood as a potential that controls the exchange of particles with the gas outside the trapped cloud by assuming that the cloud is a grand-canonical ensemble of atoms. Then the value of μ fixes the number of bosonic atoms in equilibrium.

The results of the SB approach can be compared with those of the Bogoliubov approach in the regime of a dilute condensate. The quasiparticle spectrum of a homogeneous condensate with condensate density n_0 reads [8]

$$E_{\mathbf{k}} = \sqrt{\epsilon_{\mathbf{k}}\,(2\,g n_0 + \epsilon_{\mathbf{k}})}. \tag{5}$$

The two approaches are distinguished by the parameter g, which is the interaction constant of the weakly interacting Bose gas g in the Bogoliubov approach and a renormalized effective interaction in the case of the SB approach. In the latter g is a function of the chemical potential μ and the temperature with a maximum at $\mu = 0$ [7]. Thus, for $\epsilon_{\mathbf{k}} = \hbar^2 k^2/2m$ the sound velocity reads $v_s = \sqrt{g n_0/m}$. Moreover, the healing length can also be extracted from the fluctuations of the SB approach as $\xi = \hbar/\sqrt{2mgn_0}$ [8], which also agrees with the result of the Bogoliubov approach. This means that the sound velocity and the healing length of the strongly interacting Bose gas are renormalized in comparison with the weakly interacting Bose gas. The behavior of the condensate density and the renormalized interaction parameters of the SB approach are depicted in Figs. 2, 3, respectively.

The obstacle is included by choosing specific boundary conditions for the macroscopic wave function. In our case this is a hard disk, where the wavefunction vanishes inside the disk. Finally, the number of condensed bosons N_0 is determined by an integral of $|\Phi(\mathbf{r})|^2$ over the entire volume of a three-dimensional Bose gas as

$$N_0 = \frac{1}{a^3}\frac{1}{(1+1/\alpha)^2}\int |\Phi(\mathbf{r})|^2 d^3r. \tag{6}$$

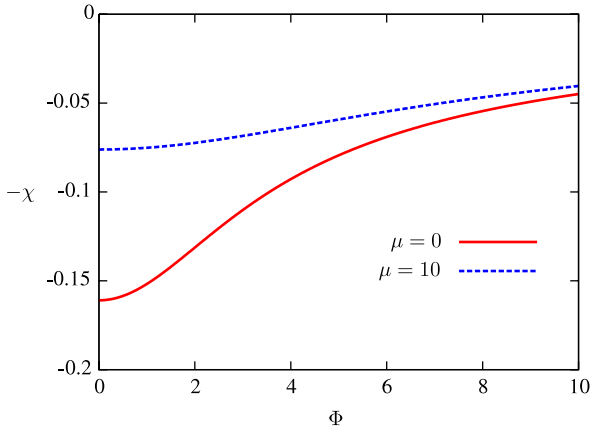

Fig. 1. Behavior of the nonlinear term $-\chi$ in Eq. (2) as a function of $|\Phi|$ for $\mu = 0$ and $\mu = 10$.

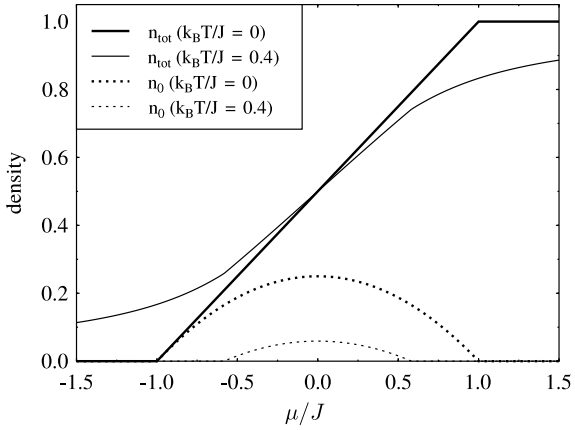

Fig. 2. The total bosonic density (full curves) and the condensate density (dashed curves) as functions of the chemical potential in the SB approach.
Source: From Ref. [8].

2.1. The nonlinear term in SIG and GP

The form of the nonlinear term χ is crucial for the physics of the strongly interacting Bose gas and makes all the difference in comparison to the GP approach. Despite the fact that it is defined in the integral representation of Eqs. (2), (3), and (4), the interpretation of its asymptotic behavior is relatively simple. First of all, this term can be expanded for low condensate density (i.e. for small Φ) to get

$$\chi \sim \chi(0) + \chi'(0)|\Phi|^2 \tag{7}$$

with $\chi'(0) < 0$ [7]. The increasing behavior of this term with $|\Phi|^2$ reflects the repulsive nature of the interaction between the bosons. The truncation after the quadratic term $|\Phi|^2$ leaves us with the Gross–Pitaevskii Hamiltonian. In the opposite limit, i.e. for $|\Phi| \sim \infty$, we get

$$\chi \sim \text{const.}\, |\Phi|^{-1}.$$

The behavior of $-\chi$ as a function of $|\Phi|^2$ is shown in Fig. 1 for two different values of the chemical potential μ. The nonlinearity is obviously much weaker than that of the GP equation. Moreover, it becomes weaker with increasing μ (i.e. increasing density of the Bose gas). This reflects the depletion of the condensate for increasing densities.

2.2. Dynamics of the macroscopic wave function

The dynamics of the quantum state of the condensate is given by the nonlinear Schrödinger equation:

$$i\hbar \frac{\partial \Phi(\mathbf{r}, t)}{\partial t} = H_\Phi \Phi(\mathbf{r}, t) = -\frac{Ja^2}{6} \Delta\Phi(\mathbf{r}, t) + J(\alpha_1 - \alpha_2 \chi)\, \Phi(\mathbf{r}, t), \tag{8}$$

which will be called SIG equation. This differential equation describes the expansion of the condensed part of a bosonic cloud for a given initial state $\Phi(\mathbf{r}, 0)$ at time $t = 0$. The spatial scale is given by scattering length $a_s \sim a$. A typical experimental value for ^{85}Rb atoms near a Feshbach resonance is $a_s \sim 200$ nm [7]. It should be noticed that the SIG equation becomes the GP equation for a low-density condensate due to Eq. (7).

3. Numerical solution and results

To study the evolution of an initial state $\Phi(\mathbf{r}, t = 0)$ with Eq. (8) we assume a two-dimensional (2D) situation, where the expansion is possible in the x, y direction but not in the z direction. This is a typical case in which the trapping potential, after the formation of the BEC, is switched off in two directions but a strongly confining potential is kept in the perpendicular direction. Then we choose for the initial state a 2D Gaussian function by

$$\Phi(x, y, t = 0) = \sqrt{\sigma_1}\, \exp\left[-0.5\, \frac{(x^2 + y^2)}{\sigma_2^2}\right], \tag{9}$$

where σ_1 and σ_2 are parameters which determine the shape of the Gaussian.

We apply a 2D finite-difference method (Crank–Nicolson method) combined with a split-step method to solve Eq. (8)

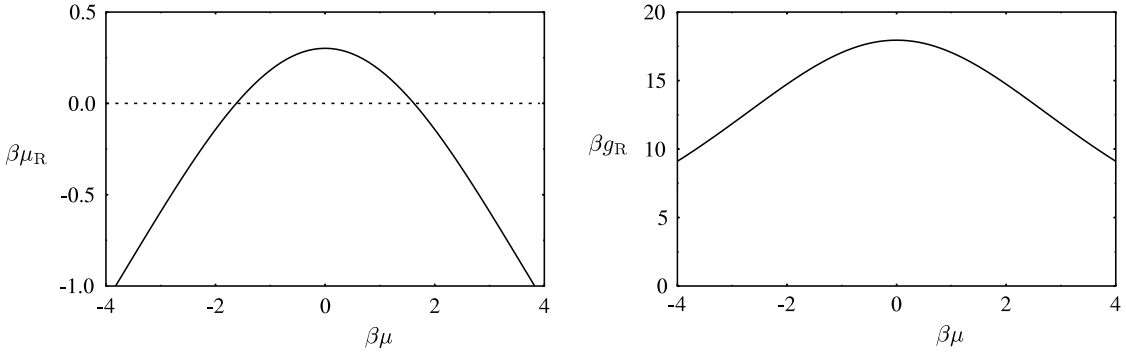

Fig. 3. Renormalized chemical potential and interaction strength of the SB approach as function of the bare chemical potential.
Source: From Ref. [8].

numerically. Schematically this reads

$$\begin{aligned}\Phi(x,y,t) &= e^{-iHt}\,\Phi(x,y,0)\\ &\approx e^{-iV\frac{\delta t}{2}}\,e^{-iT\delta t}\,e^{-iV\frac{\delta t}{2}}\,\Phi(x,y,0)\\ &\approx e^{-iV\frac{\delta t}{2}}\,\mathcal{CN}\quad y,\frac{\delta t}{2}\quad \mathcal{CN}\,[x,\delta t]\;\mathcal{CN}\quad y,\frac{\delta t}{2}\\ &\quad\times e^{-iV\frac{\delta t}{2}}\,\Phi(x,y,0)\end{aligned}\tag{10}$$

where V and T are the potential and kinetic term, respectively, δt is the time step and $\mathcal{CN}[x,\delta t]$ is the action of the Crank–Nicolson method for the kinetic term on the x direction. This approach is accurate up to $\mathcal{O}(\delta t^3)$, and good results are obtained for sufficiently small time step δt. We use a Gauss–Hermite quadrature to calculate at each time step the integrals χ and $Z(\mathbf{r})$ in (2) and (3), respectively, and notice that the Gauss–Hermite integration converges already for only nine points.

In our simulations, we use as boundary condition $\Phi(\mathbf{r}) = 0$ at the boundary of a square region. An impenetrable obstacle is implemented by assuming that the order parameter vanishes inside a circle of radius $r = 1$. The obstacle can also be implemented as a strong repulsive Gaussian potential $U(\mathbf{r}) = U_0 \exp(-(x^2+y^2)/2\kappa)$ with the chemical potential in Eq. (4) given by $\mu(\mathbf{r}) = \mu - U(\mathbf{r})$. Both conditions give similar results.

It was shown in [11] that the flow of a dilute BEC past an obstacle generates vortices and antivortices at subsonic velocity. Increasing the flow velocity, the frequency of vortices generation also increases. For large enough flow velocity, the generation of vortices is so frequent that the distance between individual vortices becomes less than their radial size and it takes a long time for their separation from each other at finite distance from the obstacle [12–14,17]. We study this transition from the generation of vortices to the generation of dark solitons in a dense Bose gas, considering different profiles of the initial state (different values of σ_1 and σ_2 in Eq. (9)). The latter corresponds to a faster expansion for a small initial profile and to a slower expansion for a bigger initial profile. There is also an effect of the chemical potential μ on the profile of the expanding cloud, as shown in Fig. 6: the width of the cloud grows with μ for negative values, reaches its maximum at $\mu = 0$ and decreases as μ increases further. This can be understood as an effect of a coupling between the condensate and the non-condensed part of the Bose gas. Although the latter has not been explicitly included in our dynamics, it affects the condensate through the μ dependence of the nonlinear term [5–8]. The condensate fraction reaches its maximum at $\mu = 0$. Consequently, the size of the BEC has its maximum at this value. This describes the effect of the non-condensed part on the BEC in our SIG equation. The GP equation, on the other hand, does not show any dependence on the chemical potential because it is completely decoupled from the non-condensed part of the Bose gas. (The chemical potential μ adds only a phase to the macroscopic wave function in the GP equation.)

We observe the emergence of pairs of vortices and antivortices using $\sigma_1 = 16$ and $\sigma_2 = \sqrt{3}\sigma_1$ in Eq. (9) (cf. Fig. 4). This is similar to what was found in recent experiments [22]. A faster expansion of the BEC can be seen for the initial state in Eq. (9) with $\sigma_1 = \sigma_2 = 8$ and different values of μ, namely $\mu = -1$, $\mu = 0$, $\mu = 1$, $\mu = 2$, $\mu = 10$ and $\mu = 20$. We observe in Figs. 5–8 a pair of oblique dark solitons past the obstacle and linear waves, as in the case of GP [14]. For small values of chemical potential, $\mu = -1$, $\mu = 0$, $\mu = 1$, $\mu = 2$, the pattern (position, slope and amplitude of the soliton) is almost the same (cf. Fig. 6). However, we find that the velocity of the expansion of the cloud becomes smaller for an increasing chemical potential (see Figs. 7 and 8).

We also study the effect of the nonlinear term χ in Eq. (2) with the full potential of Eq. (8) for different values of μ on the

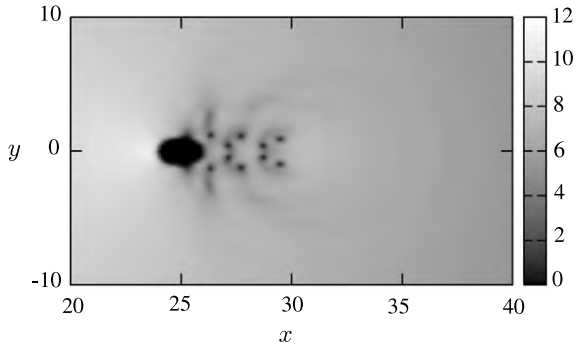

Fig. 4. Numerical solution of Eq. (8) for the initial profile given in Eq. (9) with $\sigma_1 = 16$ and $\sigma_2 = \sqrt{3}\sigma_1$. The density plot is shown for $t = 2$ and $\mu = 0$. We observe the generation of pairs of vortices and antivortices past the obstacle. An impenetrable disk of radius $r = 1$ is placed at (25, 0) in a BEC radially expanding from the center (0, 0).

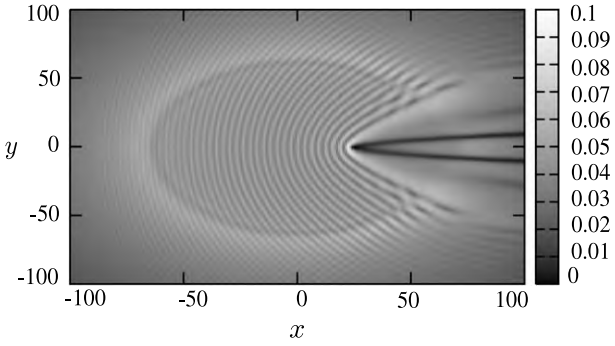

Fig. 5. Numerical solution of Eq. (8) for the initial profile given in Eq. (9) with $\sigma_1 = \sigma_2 = 8$. The density plot is shown for $t = 2$ and $\mu = 0$. The dark "V" structure corresponds to a pair of oblique dark solitons and the oscillation in front of the obstacle corresponds to the "ship" waves. An impenetrable disk of radius $r = 1$ is placed at (25, 0) in a BEC radially expanding from the center (0, 0).

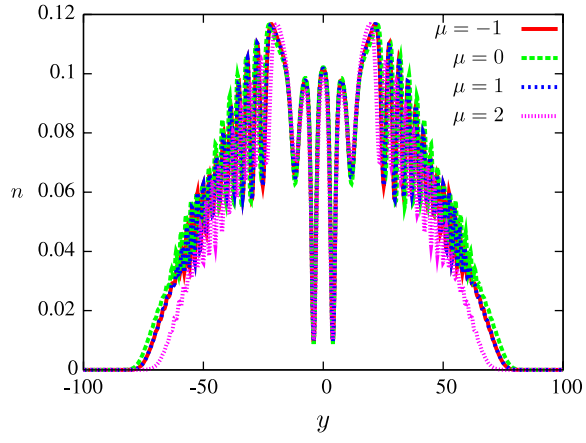

Fig. 6. Cross sections of the density distributions for $t = 2$ at $x = 60$ for chemical potential $\mu = -1$, $\mu = 0$, $\mu = 1$ and $\mu = 2$. The profile for different small μ is almost the same. However, it should be noticed that the width of the cloud is maximal for $\mu = 0$, when the condensate fraction has its maximum.

dynamics. Since χ becomes smaller as we increase μ (see Fig. 9), the expansion velocity of the cloud is also reduced with increasing μ. Correspondingly, the effective potential term of the Hamiltonian is strongly repulsive for small μ and becomes flat for bigger μ (see Fig. 10).

Although the nonlinearity of the SIG equation is more complex than its counterpart in the GP equation, the flow past an obstacle shows qualitatively the same patterns as for the GP equation: it is characterized by oblique dark solitons and by linear waves. Our

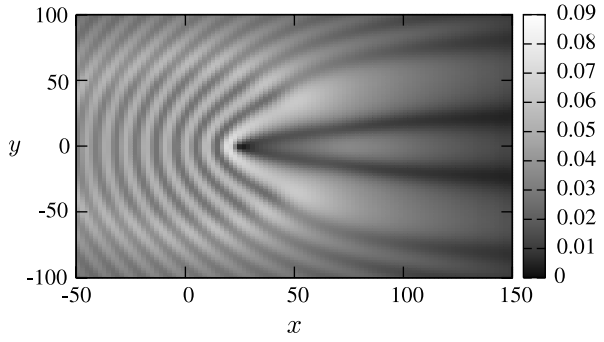

Fig. 7. Numerical solution of Eq. (8) for the initial profile given in Eq. (9) with $\sigma_1 = \sigma_2 = 8$. The density plot is shown for $t = 6$ and $\mu = 10$. The dark "V" structure corresponds to a pair of oblique dark solitons and the oscillation in front of the obstacle corresponds to the "ship" waves. An impenetrable disk of radius $r = 1$ is placed at $(25, 0)$ in a BEC radially expanding from the center $(0, 0)$.

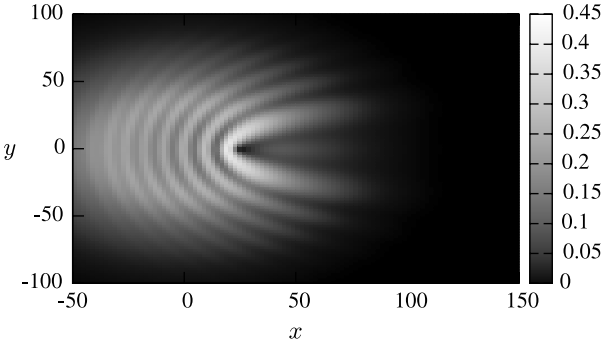

Fig. 8. Numerical solution of Eq. (8) for the initial profile given in Eq. (9) with $\sigma_1 = \sigma_2 = 8$. The density plot is shown for $t = 6$ and $\mu = 20$. The dark "V" structure corresponds to a pair of oblique dark solitons and the oscillation in front of the obstacle corresponds to the "ship" waves. An impenetrable disk of radius $r = 1$ is placed at $(25, 0)$ in a BEC radially expanding from the center $(0, 0)$. We see that for bigger μ, the expansion of the BEC is much slower than in the case illustrated in Fig. 7.

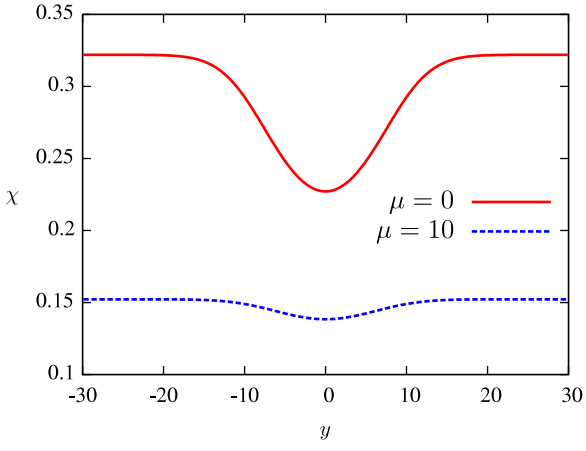

Fig. 9. Cross section at $x = 0$ of the nonlinear term χ in Eq. (2) for $\mu = 0$ and $\mu = 10$. It goes to zero as we increase μ.

study suggests that these effects shall well appear in a strongly interacting gas too and may be observed experimentally.

4. Conclusion

We have studied the two-dimensional expansion of a strongly interacting BEC in the presence of an obstacle. The strong interaction was treated within the slave-boson approach, which leads

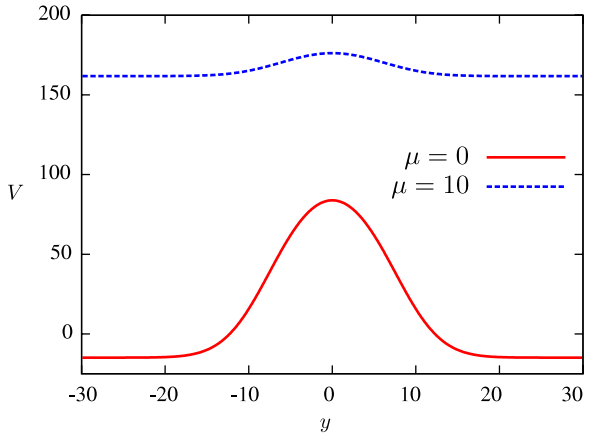

Fig. 10. Cross section at $x = 0$ of the potential term in Eq. (8) for $\mu = 0$ and $\mu = 10$. It becomes flat as we increase μ. It makes the expansion of the cloud slower for big μ.

to a nonlinear Schrödinger equation with a special nonlinearity, different from the Gross–Pitaevskii term. We solved numerically this equation and analyzed the contribution of the nonlinearity. Similar to what was found in previous studies of the GP equation [11,14], we observed the pairwise generation of vortices and antivortices (at low velocity) and of shock waves (at high velocity), respectively. We noticed that bigger values of the chemical potential (i.e. for higher densities of the Bose gas) the expansion is slower due to a reduced nonlinear term. The characteristic features of the SIG equation in terms of a generation of vortices, oblique dark solitons and ship waves are similar to those described by the GP. However, in contrast to the results of the GP equation, the densities of the SIG vary with the chemical potential μ.

Acknowledgments

This work was supported by Coordenação de Aperfeiçoamento de Pessoal de Nível Superior (CAPES/PROBRAL 225/06) and Deutscher Akademischer Austausch Dienst (DAAD). AG also thanks Brazilian funding agencies FAPESP (2011/18998-2) and CNPq (304468/2014-2).

References

[1] Franco Dalfovo, Stefano Giorgini, Lev P. Pitaevskii, Rev. Modern Phys. 71 (1999) 463–512.
[2] Oliver Morsch, Markus Oberthaler, Rev. Modern Phys. 78 (2006) 179–215.
[3] Several articles in Quantum Gases: Finite Temperature and Non-Equilibrium Dynamics, Ed. Proukakis et al., Imperial College Press (2013).
[4] N.P. Proukakis, B. Jackson, J. Phys. B 41 (2008) 203002.
[5] K. Ziegler, A. Shukla, Phys. Rev. A 56 (1997) 1438.
[6] K. Ziegler, Laser Phys. 12 (2002) 1.
[7] Ch. Moseley, K. Ziegler, J. Phys. B 40 (2007) 629.
[8] Ch. Moseley, O. Fialko, K. Ziegler, Ann. Phys. (Berlin) 17 (8) (2008) 561.
[9] V.P. Barros, Ch. Moseley, A. Gammal, K. Ziegler, Phys. Rev. A 78 (2008) 013642.
[10] L. Pitaevskii, S. Stringari, Bose Einstein Condensation, Clarendon Press, Oxford, 2003.
[11] T. Frisch, Y. Pomeau, S. Rica, Phys. Rev. Lett. 69 (1992) 1644.
[12] T. Winiecki, J.F. McCann, C.S. Adams, Phys. Rev. Lett. 82 (1999) 5186.
[13] T. Winiecki, B. Jackson, J.F. McCann, C.S. Adams, J. Phys. B: At. Mol. Opt. Phys. 33 (2000) 4069.
[14] G.A. El, A. Gammal, A.M. Kamchatnov, Phys. Rev. Lett. 97 (2006) 180405.
[15] Yu.G. Gladush, G.A. El, A. Gammal, A.M. Kamchatnov, Phys. Rev. A 75 (2007) 033619.
[16] G.A. El, A. Gammal, A.M. Kamchatnov, Nuclear Phys. A 790 (2007) 771c.
[17] A.M. Kamchatnov, L.P. Pitaevskii, Phys. Rev. Lett. 100 (2008) 160402.
[18] G.A. El, A.M. Kamchatnov, V.V. Khodorovskii, E.S. Annibale, A. Gammal, Phys. Rev. E 80 (2009) 046317.
[19] D.J. Frantzeskakis, J. Phys. A 43 (2010) 213001.
[20] E.A. Cornell, Conference on Nonlinear Waves, Integrable Systems and their Applications, Colorado Springs, 2005. http://jilawww.colorado.edu/bec/papers.html.
[21] I. Carusotto, S.X. Hu, L.A. Collins, A. Smerzi, Phys. Rev. Lett. 97 (2006) 260403.
[22] T.W. Neely, E.C. Samson, A.S. Bradley, M.J. Davis, B.P. Anderson, Phys. Rev. Lett. 104 (2010) 160401.
[23] K. Sasaki, N. Suzuki, H. Saito, Phys. Rev. Lett. 104 (2010) 150404.